X-ray absorption and resonant inelastic x-ray scattering in the rare earths

Michel van Veenendaal* and Robert Benoist
European Synchrotron Radiation Facility, Boîte Postale 220, F-38043 Grenoble Cédex, France
(Received 25 February 1997; revised manuscript received 10 March 1998)

This paper makes a comparison between x-ray absorption (XAS) and resonant inelastic x-ray scattering (RIXS) in the rare earths. Atomic calculations are given for $2p \rightarrow 4f$. The radiative decay of the XAS final states is described for the situations where the core hole created in the absorption process is filled by a valence electron or by an electron from a shallower core level. RIXS spectra $4f^n \rightarrow \underline{3d}4f^{n+1} \rightarrow 4f^n$ integrated over the outgoing photon energy (fluorescence yield) are compared with $3d \rightarrow 4f$ XAS. Sum rules related to XAS and RIXS and their applicability are discussed. [S0163-1829(98)06631-4]

I. INTRODUCTION

Experiments on rare-earth systems have made a significant contribution to the development of magnetic x-ray dichroism and resonant magnetic scattering. Important circular[1] and linear[2] magnetic x-ray dichroism experiments have been performed on rare earths. The first satisfactory explanation of resonant magnetic scattering was done for holmium metal.[3,4] The electronic structure of rare earths is determined by the interaction between electrons in the localized $4f$ orbitals and in the broad $5d$ band. Spectroscopies involving the $4f$ shell can usually be successfully described by atomic multiplet theory. However, whereas, e.g., magnetic x-ray dichroism at the M_{45} edges is rather well understood, the L_{23} spectra, dominated by the dipolar $2p \rightarrow 5d$ transitions, pose more problems. In the interpretation one has to take into account two effects.

First, one observes pre-edge features[5,6] that are weak in the isotropic spectra but have a strong circular dichroic signal. That these structures arise from quadrupolar transitions into the $4f$ shell has been established by resonant elastic $\sigma \rightarrow \pi$ x-ray scattering,[3,4] by the observation of a nondipolar angular dependence of the circular dichroic x-ray absorption (XAS),[7,8] by resonant Raman spectroscopy,[9,10] and by partial deconvolution of the lifetime broadening.[11]

Second, the finite integrated intensity of the circular dichroism of the $2p \rightarrow 5d$ transitions results not only from the polarization of the $5d$ electrons in the ground state but also from a dependence of the $2p$-$5d$ radial matrix elements on the direction of the $5d$ moment relative to that of the $4f$.[7,12] Therefore, band effects[7] and the full df-Coulomb interaction[13,14] have to be included in the interpretation of the spectral line shape and the variations in the L_{23} circular dichroic branching ratios.

A complication in the interpretation of resonant inelastic x-ray scattering (RIXS) is that the deexcitation cannot be simply decoupled from the absorption step as can be done when the excitation is far above threshold. Furthermore, the decay is different for transitions between two core levels or between the valence shell and a core level.

For systems where a detailed description of the spectral line shape is complex, useful results can still be obtained from statistical methods. For XAS and x-ray scattering sum rules exist that relate the integrated intensities to ground state properties.[15–18] These sum rules rely on a number of approximations. In general, a constant radial matrix element is required. For sum rules that consider the spin-orbit manifolds separately one has to assume that the edges can be distinguished by the j value of the core hole. For fluorescence yield no exact sum rules have been derived so far and the application of XAS sum rules requires numerical validation.[19] In this paper we address the applicability of the sum rules.

The paper is divided as follows. First, in Sec. II, we show the separation of the geometric and dynamical part for XAS and RIXS. We make use of spherical tensor algebra, which enables a general treatment for different transition operators and different polarization geometries. In order to obtain nicely normalized quantities we make extensive use of normalization constants that remove the square roots from the expressions and lead to a geometric part that is unity in the isotropic case. These square roots are a result of the normalization of the $3j$ symbols and are inconvenient when dealing with physical quantities such as operators and spectra. Section III gives a derivation for the angular distributions for some common experimental situations. Section IV is devoted to the spectral functions and their sum rules. We describe the spectral line shape of the XAS spectra at the L_{23} edge. RIXS results are discussed for spectroscopies involving the $4f$ shell. A comparison is made between the radiative decay in spectroscopies where the intermediate state core hole is filled by a valence electron or by an electron from a shallower core level. We end with a conclusion in Sec. V.

II. INTENSITIES

The intershell transitions as a result of the absorption or emission of a x-ray photon are described by $H_{\rm int} = (e/2m)(\mathbf{p}\cdot\mathbf{A}+\mathbf{A}\cdot\mathbf{p})$. Expanding the vector potential in plane waves gives

$$\mathbf{A} = \sum_{\mathbf{k},\boldsymbol{\epsilon}} \sqrt{\frac{\hbar}{2\omega\epsilon_0\Omega}} (\boldsymbol{\epsilon} a_{\mathbf{k}\boldsymbol{\epsilon}} e^{i\mathbf{k}\cdot\mathbf{r}} + \text{H.c.}), \tag{1}$$

where Ω is a normalization volume and $a_{\mathbf{k}\boldsymbol{\epsilon}}$ annihilates a photon with momentum $\mathbf{k}$ and polarization vector $\boldsymbol{\epsilon}$. The absorption intensity is then given by Fermi's golden rule

TABLE I. Relevant constants for electric dipole ($tQ=01$), magnetic dipole ($tQ=11$), and electric quadrupole ($tQ=12$) transitions. The factors $b_{tQ}(k)$ appear in the definition of the operators $\mathbf{V}^{tQ}$. The B_Q^2 give the relative probabilities of dipolar and quadrupolar transitions. The factors D_{tQ} are used in the definition of the angular dependence $\mathbf{T}^{tQz}$.

Transition	t	Q	$\mathbf{V}^{tQ}$	$b_{tQ}(k)$	B_Q^2	D_{tQ}
Electric dipole	0	1	$\mathbf{r}$	$\sqrt{3}$	$\frac{1}{3}$	3
Magnetic dipole	1	1	$\frac{\alpha}{2}\frac{a_0}{\hbar}\mathbf{L}$	$\sqrt{\frac{3}{2}}k$	$\frac{1}{3}$	$3\sqrt{2}$
Electric quadupole	1	2	$\mathbf{r}^{(2)}$	$-\sqrt{30}$	$\frac{1}{15}\left(\frac{k}{2}\right)^2$	$-5\sqrt{2}$

$$I(\hat{\mathbf{k}}\boldsymbol{\epsilon}\omega)=\frac{2\pi}{\hbar}\sum_n |\langle n|H_{\rm int}|g\rangle|^2\delta(\omega+E_g-E_n)\rho_\omega, \quad (2)$$

with the density of oscillators given by $\rho_\omega=(\Omega/8\pi^3)(\omega^2/\hbar c^3)$. The different multipoles[20] of the spectrum are obtained by expanding the plane wave in Bessel functions and spherical harmonics, i.e.,

$$e^{i\mathbf{k}\cdot\mathbf{r}}=\sum_t [t] i^t j_t(kr)\hat{\mathbf{k}}^{(t)}\cdot\hat{\mathbf{r}}^{(t)}, \quad (3)$$

with $[a\cdots b]=(2a+1)\cdots(2b+1)$. The tensor products in this paper are done with $3j$ symbols, which are up to a factor equivalent to those with Clebsch-Gordan coefficients,

$$[\mathbf{a}^l,\mathbf{b}^{l'}]^x_\xi=\sum_{\lambda,\lambda'} a^l_\lambda b^{l'}_{-\lambda'}(-1)^{l-\lambda-\lambda'}\begin{pmatrix} l & x & l' \\ -\lambda & \xi & \lambda' \end{pmatrix}$$

$$=(-1)^{l'}[x]^{-1/2}\sum_{\lambda,\lambda'} a^l_\lambda b^{l'}_{\lambda'} C^{x\xi}_{l\lambda,l'\lambda'}, \quad (4)$$

where $\mathbf{a}^l$ is a spherical tensor of rank l and a^l_λ are its components; a tensor without a superscript has rank one. The inner product is given by $[\mathbf{a}^l,\mathbf{b}^l]^0_0[l]^{1/2}=\mathbf{a}^l\cdot\mathbf{b}^l$. We use here the shorthand notation $\mathbf{k}^{(l)}=k^l\mathbf{C}^l(\hat{\mathbf{k}})$, with $C^l_m(\hat{\mathbf{k}})=\sqrt{4\pi/(2l+1)}Y^l_m(\hat{\mathbf{k}})$;[21] for spherical tensors of rank one $\mathbf{k}=\mathbf{k}^{(1)}$. Note that $\hat{k}=1$. For $kr\ll 1$ one has $j_t(kr)\cong(kr)^t/[t]!!$. With the use of

$$(\mathbf{a}^l\cdot\mathbf{b}^l)(\mathbf{c}^{l'}\cdot\mathbf{d}^{l'})=\sum_x [x][\mathbf{a}^l,\mathbf{c}^{l'}]^x\cdot[\mathbf{b}^l,\mathbf{d}^{l'}]^x \quad (5)$$

one then obtains

$$\mathbf{p}\cdot\boldsymbol{\epsilon}\, e^{i\mathbf{k}\cdot\mathbf{r}}=\sum_{tQ}[tQ]\frac{i^t}{[t]!!}[\mathbf{p},\mathbf{r}^{(t)}]^Q\cdot[\boldsymbol{\epsilon},\mathbf{k}^{(t)}]^Q. \quad (6)$$

It is convenient to define the operators

$$\mathbf{V}^{tQ}=\frac{b_{tQ}(k)}{2im\omega}\{[\mathbf{p},\mathbf{r}^{(t)}]^Q+(-1)^Q[\mathbf{r}^{(t)},\mathbf{p}]^Q\}, \quad (7)$$

where the factors $b_{tQ}(k)$ will be chosen in such a way that nicely defined operators are obtained; see Table I. For $tQ=01$ (electric dipole) and $b_{01}(k)=\sqrt{3}$ we have

$$\langle n|\mathbf{V}^{01}|g\rangle=\frac{b_{01}(k)}{\sqrt{3}im\omega}\langle n|\mathbf{p}|g\rangle=\frac{1}{\hbar\omega}\left\langle n\left|\left[\frac{p^2}{2m},\mathbf{r}\right]\right|g\right\rangle$$

$$\cong\langle n|\mathbf{r}|g\rangle. \quad (8)$$

By using the definition for the outer product $[\mathbf{a},\mathbf{b}]^1=-(i/\sqrt{6})\mathbf{a}\times\mathbf{b}$ and $b_{11}(k)=\sqrt{\frac{3}{2}}k$, we find that $\mathbf{V}^{11}$ is equal to $[b_{11}(k)/im\omega][\mathbf{p},\mathbf{r}]^1=(\alpha/2)(a_0/\hbar)\mathbf{L}$, with α the fine-structure constant and a_0 the Bohr radius. $\mathbf{V}^{11}$ forms together with the $g_S\mathbf{S}$ term the magnetic dipole operator. Magnetic dipole transitions are about $(\alpha/2)^2$, i.e., five orders of magnitude smaller than electric dipole transitions of the same wavelength. Furthermore, we have for the electric quadrupole operator $\mathbf{V}^{12}=\mathbf{r}^{(2)}$ that $b_{12}(k)=\sqrt{30}$.

The multipole expansion enables us to separate the absorption intensity into a geometric and an electronic part, i.e.,

$$I(\hat{\mathbf{k}}\boldsymbol{\epsilon}\omega)=\frac{2\pi}{\hbar}N_\omega\sum_{t,Q,n} B_Q^2 D_{tQ}^2|\langle n|[\boldsymbol{\epsilon},\mathbf{k}^{(t)}]^Q\cdot\mathbf{V}^{tQ}|g\rangle|^2$$

$$\times\delta(\omega+E_g-E_n)$$

$$=\frac{2\pi}{\hbar}N_\omega\sum_{t,Q,z} B_Q^2\mathbf{T}^{tQz}(\hat{\mathbf{k}}\boldsymbol{\epsilon})\cdot\mathbf{I}^{tQz}(\omega), \quad (9)$$

where we have applied Eq. (5). The cross terms between different tQ values have been omitted. The following factors have been defined: $N_\omega=e^2\omega^3/16\pi^3\epsilon_0c^3$; $B_Q=(k/2)^{Q-1}([Q]!!)^{-1/2}$ gives the relative transition probability, where for the dipolar and quadrupolar contributions one has $B_2^2/B_1^2=\frac{1}{5}(k/2)^2$; and $D_{tQ}=[tQ]k^t/[t]!!b_{tQ}(k)B_Q$. The different multipole spectra are given by

$$\mathbf{I}^{tQz}(\omega)=\frac{\Gamma}{\pi}\sum_n\frac{1}{|\mathcal{E}_n|^2}\mathbf{I}^{tQz}(gnng), \quad (10)$$

with $\mathcal{E}_n=\omega+E_g-E_n+i(\Gamma/2)$ where Γ is the lifetime broadening of the XAS final states; the different combinations of the matrix elements are defined as

$$\mathbf{I}^{tQz}(abcd)=[\langle a|(\mathbf{V}^\dagger)^{tQ}|b\rangle,\langle c|\mathbf{V}^{tQ}|d\rangle]^z n_{Qz}^{-1}, \quad (11)$$

where the normalization constants n_{Qz} are defined as

$$n_{lx}=\begin{pmatrix} l & x & l \\ -l & 0 & l \end{pmatrix}=\frac{(2l)!}{\sqrt{(2l-x)!(2l+1+x)!}}. \quad (12)$$

The angular distribution is given by

$$\mathbf{T}^{tQz}(\hat{\mathbf{k}}\boldsymbol{\epsilon})=[z]D_{tQ}^2[[\boldsymbol{\epsilon}^*,\hat{\mathbf{k}}^{(t)}]^Q,[\boldsymbol{\epsilon},\hat{\mathbf{k}}^{(t)}]^Q]^z n_{Qz}. \quad (13)$$

$\mathbf{T}^{tQz}$ weighs the different spectra $\mathbf{I}^{tQz}(\omega)$ as a function of the wave vector $\hat{\mathbf{k}}$ and the polarization vector $\boldsymbol{\epsilon}$ of the incoming light.

The RIXS intensity is proportional to

$$I(\hat{\mathbf{k}}\boldsymbol{\epsilon}\omega,\hat{\mathbf{k}}'\boldsymbol{\epsilon}'\omega')=\frac{2\pi}{\hbar}\sum_f\left|\sum_n\frac{\langle f|H_{\rm int}|n\rangle\langle n|H_{\rm int}|g\rangle}{\omega+E_g-E_n+i(\Gamma/2)}\right|^2$$

$$\times\delta(\omega+E_g-\omega'-E_f)\rho_{\omega'}\rho_\omega. \quad (14)$$

TABLE II. Bipolar spherical harmonic $U^{xyz}(\mathbf{a},\mathbf{b},\mathbf{c})$ relevant for the angular dependence of dipolar transitions.

$U^{110}=\mathbf{a}\cdot\mathbf{b}$
$U^{111}=\frac{2}{3}(\mathbf{a}\times\mathbf{b})\cdot\mathbf{c}$
$U^{112}=\frac{3}{2}(\mathbf{a}\cdot\mathbf{c})(\mathbf{b}\cdot\mathbf{c})-\frac{1}{2}(\mathbf{a}\cdot\mathbf{b})$

In the remainder of the paper we consider the different multipole transitions separately; to reduce the number of indices we suppress the tQ of the transitions. In a way similar to that for XAS we find for the RIXS cross section with Q-polar excitation followed by a Q'-polar deexcitation

$$I(\hat{\mathbf{k}}\boldsymbol{\epsilon}\omega,\hat{\mathbf{k}}'\boldsymbol{\epsilon}'\omega')=\frac{2\pi}{\hbar}N_{\omega'}B_{Q'}^2N_{\omega}B_Q^2 \times\sum_{z,z',r}\mathbf{T}^{zz'r}(\hat{\mathbf{k}}\boldsymbol{\epsilon},\hat{\mathbf{k}}'\boldsymbol{\epsilon}')\cdot\mathbf{I}^{zz'r}(\omega,\omega'). \tag{15}$$

The dynamical part has now become a tensor product of absorption and emission

$$\mathbf{I}^{zz'r}(\omega,\omega')=[r]\frac{\gamma}{\pi}\sum_{n,n',f}\frac{1}{|\mathcal{E}_f|^2}\frac{1}{\mathcal{E}_{n'}^*\mathcal{E}_n}\times[\mathbf{I}^{z'}(n'ffn),\mathbf{I}^{z}(gn'ng)]^r n_{zz'r}, \tag{16}$$

where $\mathcal{E}_f=\omega+E_g-\omega'-E_f+i(\gamma/2)$, with γ the lifetime broadening of the x-ray inelastic scattering final states. The normalization constant n_{xyz} is defined as

$$n_{xyz}=\begin{pmatrix}x & y & z\\ 0 & 0 & 0\end{pmatrix}. \tag{17}$$

n_{xyz} is zero for odd $x+y+z$. We also use $\underline{n}_{xyz}$, which is complex for odd $x+y+z$ and equal to n_{xyz} for even $x+y+z$.[22] The angular dependence is given by

$$\mathbf{T}^{zz'r}(\hat{\mathbf{k}}\boldsymbol{\epsilon},\hat{\mathbf{k}}'\boldsymbol{\epsilon}')=[\mathbf{T}^{z'}(\hat{\mathbf{k}}'\boldsymbol{\epsilon}'),\mathbf{T}^{z}(\hat{\mathbf{k}}\boldsymbol{\epsilon})]^r n^{-1}_{zz'r}. \tag{18}$$

III. ANGULAR DEPENDENCE

The tensors for the angular dependence are chosen in such a way that $\mathbf{T}^0=1$ for $tQ=01,11,12$. For electric dipole transitions $\mathbf{T}^z$ is $\hat{\mathbf{k}}$ independent and the $\zeta=0$ component is, with respect to the $\hat{\mathbf{Z}}$ axis of our system,

$$T_0^z(\boldsymbol{\epsilon})=3[z](-1)^{1+z}n_{Qz}n_{11z}U^{11z}(\boldsymbol{\epsilon}^*,\boldsymbol{\epsilon},\hat{\mathbf{Z}}), \tag{19}$$

where the bipolar spherical harmonics[23] are given by $U^{xyz}(\mathbf{a},\mathbf{b},\mathbf{c})=(-1)^{y+z}\underline{n}^{-1}_{xyz}[\mathbf{a}^{(x)}\mathbf{b}^{(y)}]^z\cdot\mathbf{c}^{(z)}$. The bipolar spherical harmonics with xyz relevant for dipolar transitions are given in Table II; expressions for higher values of xyz are given by Thole and van der Laan.[22] For general multipole transitions it is more convenient to recouple the angular dependence

TABLE III. Coeficients $\mathcal{T}_z$ defined in Eq. (23) for electric dipolar and quadrupolar transitions ($z=0,\ldots,2Q$).

		z				
t	Q	0	1	2	3	4
0	1	1	$\frac{3}{2}$	$\frac{1}{2}$		
1	2	1	1	$-\frac{5}{7}$	-1	$-\frac{2}{7}$

$$\mathbf{T}^z(\hat{\mathbf{k}}\boldsymbol{\epsilon})=D^2_{tQ}n_{Qz}\sum_{x,y}[xyz](-1)^{Q-1-t-y}\begin{Bmatrix}1 & t & Q\\ 1 & t & Q\\ x & y & z\end{Bmatrix}\times[[\boldsymbol{\epsilon}^*,\boldsymbol{\epsilon}]^x,[\hat{\mathbf{k}}^{(t)},\hat{\mathbf{k}}^{(t)}]^y]^z. \tag{20}$$

This form is convenient for the comparisation of light of different polarizations as it enables us to factor out the polarization vectors. For linearly polarized light with polarization vectors $\boldsymbol{\epsilon}_x$ and $\boldsymbol{\epsilon}_y$ in the x and y directions, respectively, it is straightforward to show that

$$\frac{1}{2}\{[\boldsymbol{\epsilon}_x^*,\boldsymbol{\epsilon}_x]^x+(-1)^x[\boldsymbol{\epsilon}_y^*,\boldsymbol{\epsilon}_y]^x\}=\mathrm{Re}\{a_x\}\ \underline{n}_{11x}C^x(\hat{\mathbf{k}}), \tag{21}$$

whereas for circularly polarized light, where $\boldsymbol{\epsilon}_\pm=\mp(1/\sqrt{2})(\boldsymbol{\epsilon}_x\pm i\boldsymbol{\epsilon}_y)$, we find

$$\frac{1}{2}\{[\boldsymbol{\epsilon}_+^*,\boldsymbol{\epsilon}_+]^x+(-1)^{x+m}[\boldsymbol{\epsilon}_-^*,\boldsymbol{\epsilon}_-]^x\}=\begin{cases}a_x\ \underline{n}_{11x}C^x(\hat{\mathbf{k}}), & m=0\\ 0, & m=1,\end{cases} \tag{22}$$

with $a_x=-1,\frac{2}{3}i,\frac{1}{2}$ for $x=0,1,2$. With the use of $[\mathbf{C}^l(\hat{\mathbf{k}}),\mathbf{C}^{l'}(\hat{\mathbf{k}})]^x=\mathbf{C}^x(\hat{\mathbf{k}})(-1)^l n_{ll'x}$, the angular dependence is found to be proportional to $\mathbf{C}^z(\hat{\mathbf{k}})$,[5]

$$\frac{1}{2}[\mathbf{T}^z(\hat{\mathbf{k}}\boldsymbol{\epsilon}_+)+(-1)^{z+m}\mathbf{T}^z(\hat{\mathbf{k}}\boldsymbol{\epsilon}_-)]=\begin{cases}\mathcal{T}_z\mathbf{C}^z(\hat{\mathbf{k}}), & m=0\\ 0, & m=1,\end{cases} \tag{23}$$

where the coefficients

$$\mathcal{T}_z=D^2_{tQ}(-1)^{Q-1+z}\sum_{x,y}[xyz]a_x n_{Qz}\begin{Bmatrix}1 & t & Q\\ 1 & t & Q\\ x & y & z\end{Bmatrix}\times\underline{n}_{11x}n_{tty}n_{xyz} \tag{24}$$

are given in Table III.

IV. SPECTRA AND SUM RULES

A. XAS into the 4f shell

Here we consider two absorption edges often studied: the L_{23} edges, corresponding to transitions from the $2p$ orbital into the valence shell, and the M_{45} edges, which are dominated by the dipolar $3d\rightarrow 4f$ transitions. The electric dipolar and quadrupolar transition operators are given by the Wigner-Eckart theorem

TABLE IV. Spectra I_0^z expressed in I_q for $Q=1,2$.

Q	I_0^z
1 (dipolar)	$I_0^0=I_1+I_0+I_{-1}$
	$I_0^1=I_1-I_{-1}$
	$I_0^2=I_1-2I_0+I_{-1}$
2 (quadrupolar)	$I_0^0=I_2+I_1+I_0+I_{-1}+I_{-2}$
	$I_0^1=I_2+\frac{1}{2}I_1-\frac{1}{2}I_{-1}-I_{-2}$
	$I_0^2=I_2-\frac{1}{2}I_1-I_0-\frac{1}{2}I_{-1}+I_{-2}$
	$I_0^3=I_2-2I_1+2I_{-1}-I_{-2}$
	$I_0^4=I_2-4I_1+6I_0-4I_{-1}+I_{-2}$

$$\langle n|V_q|g\rangle=P_{cl}\sum_{\gamma,\lambda,\sigma}(-1)^{l-\lambda}\begin{pmatrix} l & Q & c \\ -\lambda & q & \gamma\end{pmatrix}\langle n|l^\dagger_{\lambda\sigma}c_{\gamma\sigma}|g\rangle, \tag{25}$$

where $l^\dagger_{\lambda\sigma}$ creates an electron in shell l with orbital component λ and spin σ. The reduced matrix element is given by

$$P_{cl}(Q)=(-1)^l n_{lQc}[lc]^{1/2}\int dr\ R_{n_l l}(r)r^Q R_{n_c c}(r). \tag{26}$$

For rare earths the crystal fields on the $4f$ electrons are often negligibly small and one can assume spherical symmetry SO_3. For a magnetic system the symmetry is lowered to SO_2 and the J values branch into $M_J=-J,\ldots,J$. Here we take the magnetic axis along the $\hat{\mathbf{Z}}$ axis and the ground state to be $M_J=J$. To obtain a nonzero intensity the total transition operator has to be totally symmetric. This means we have to consider $I_0^z(\omega)$ for XAS and $I_0^{zz'r}(\omega,\omega')$ for RIXS. I_0^z is a combination of the matrix elements $I_q(gnng)=\langle g|V_q^\dagger|n\rangle\langle n|V_q|g\rangle$. The combinations for $Q=1,2$ are given in Table IV. For dipolar transitions we have the well-known spectra: isotropic (I_0^0), circular dichroic (I_0^1), and linear dichroic (I_0^2).

Figures 1–4 give the XAS spectra for transitions into the $4f$ shell at the $L_{2,3}$ and $M_{4,5}$ edges. Calculations were done in the atomic limit using Cowan's programs.[24] The Hamiltonian includes the Coulomb interactions in the $4f$ shell and those between the $4f$ shell and the core hole and the spin-orbit coupling. Parameters were obtained in the Hartree-Fock limit and the values for the Coulomb interaction were scaled down to 80% to account for screening effects. This scaling down factor produces good agreement between theory and experiment.[25] The zero of the energy scale corresponds to the energy of the lowest eigenstate in a spin-orbit manifold. Figure 1 gives the isotropic $2p\rightarrow 4f$ XAS spectrum using a Lorentzian broadening of 4 eV. Recently, Loeffen *et al.*[11] demonstrated the possibility of separating the dipolar and quadrupolar features by deconvolution of high-quality XAS data by a Lorentzian with a width of 3 eV. The resulting spectral line shape of the pre-edge structures was in agreement with multiplet calculations. This method seems to be well suited to study the relative contributions of quadrupolar and dipolar transitions. The spectrum obtained after taking

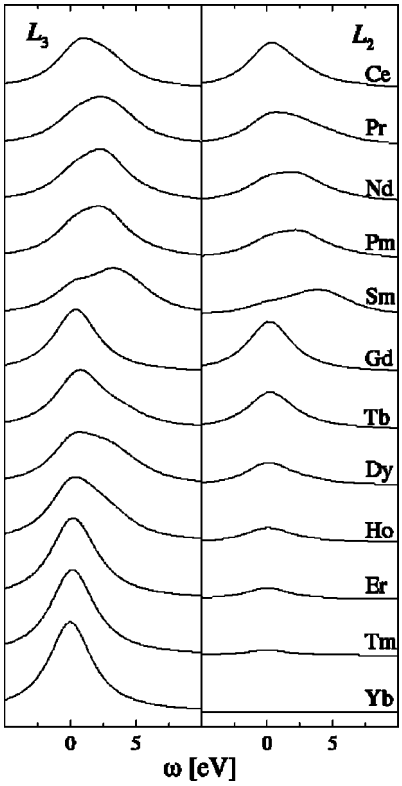

FIG. 1. Isotropic quadrupolar $2p\rightarrow 4f$ XAS spectra as a function of excitation energy ω for trivalent rare-earth ions. The left and right panels show the L_3 and L_2 edges, respectively. Spectra for the L_2 edge have been scaled by a factor 2.

the difference between left and right circularly polarized light is a combination of I_0^z with odd z. Using Eq. (23) we obtain[5]

$$\frac{1}{2}\{I(\hat{\mathbf{k}}\boldsymbol{\epsilon}^+\omega)-I(\hat{\mathbf{k}}\boldsymbol{\epsilon}^-\omega)\}=\frac{2\pi}{\hbar}N_\omega B_2^2\{-C_0^1(\hat{\mathbf{k}})I_0^1(\omega)+C_0^3(\hat{\mathbf{k}})I_0^3(\omega)\}, \tag{27}$$

where $C_0^z(\hat{\mathbf{k}})$ are Legendre polynomials of order z, i.e., $P^z(\cos\theta)$ with θ the angle between the direction of the light and the magnetic axis. The spectra $I_0^1(\omega)$ and $I_0^3(\omega)$ are given in Fig. 2.

Figures 3 and 4 show, respectively, the isotropic and circular dichroic $M_{4,5}$ XAS spectra ($\Gamma=0.8$ eV). These spectra have been published earlier[25–27] and are included for comparison with the fluorescence yield spectra.

The behavior of the intensities can be related to ground state expectation values by sum rules.[15,16,28] For $l=c+Q$ one can reduce the expressions to[29,30]

$$I_0^z(j)=\int_j d\omega\ I_0^z(\omega)=\frac{P_{cl}^2}{[cl]}\sum_{x,y}M_y(j)N_{xyz}\langle w_0^{xyz}\rangle, \tag{28}$$

with $M_y(j)=c+1,c,c,-c$ for $jy=j^+0,j^+1,j^-0,j^-1$ ($j^\pm=l\pm s$) and $N_{xyz}=1,z/[z],(z+1)/[z]$ for $xyz=z0z;\ z-1,1,z;z+1,1,z$. The coupled tensor operators are defined as[29,31]

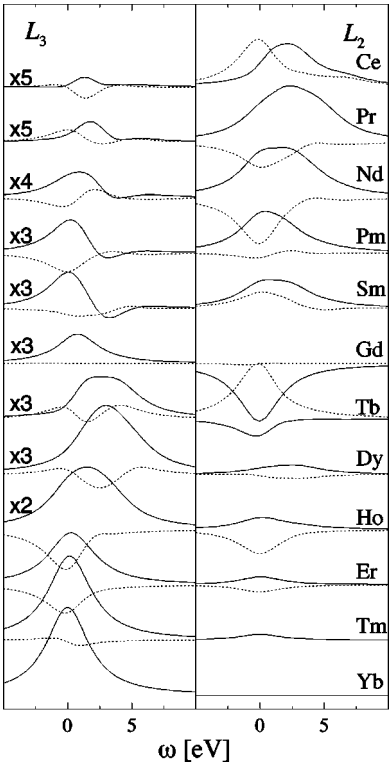

FIG. 2. Quadrupolar $2p \rightarrow 4f$ XAS spectra as a function of excitation energy ω for trivalent rare-earth ions. The spectrum for left minus right circularly polarized light is an angular-dependent combination of I^1 (solid line) and I^3 (dotted line); see the text. The left and right panels show the L_3 and L_2 edges, respectively. Spectra for the L_2 edge have been scaled by a factor 2. Furthermore, some of the spectra are scaled relatively to the spectra of Fig. 1. The scaling also applies to the right panel.

$$w_{\zeta}^{xyz} = \sum_{\lambda,\lambda',\sigma,\sigma',\xi,\eta} (-1)^{l-\lambda'+s-\sigma} \begin{pmatrix} l & x & l \\ -\lambda' & \xi & \lambda \end{pmatrix} \times \begin{pmatrix} s & y & s \\ -\sigma' & \eta & \sigma \end{pmatrix} \times (-1)^{z-\zeta} \begin{pmatrix} x & y & z \\ -\xi & -\eta & \zeta \end{pmatrix} \times l_{\lambda'\sigma'} l^{\dagger}_{\lambda\sigma} n_{lx}^{-1} n_{sy}^{-1} \underline{n}_{xyz}^{-1}, \tag{29}$$

with $s=\frac{1}{2}$. The operators are spin independent and dependent for $y=0$ and 1, respectively. These hole coupled tensor operators are related to the electron operators defined by Carra *et al.*[32] via $O^{xyz}=2[l]\delta_{x,0}\delta_{y,0}-(-1)^z r_{lx} r_{sy} w_0^{xyz}$ with $r_{lx}=(2l)!/2^x(2l-x)!$. The advantage of using normalized operators over Judd's operators[31] is that the square roots are removed from the expressions. They are normalized in such a way that the expectation values are unity for a ground state with one hole and $M_J=J=l+\frac{1}{2}$ [i.e., for rare earths the ground state of Yb^{3+}, $f^{13}(^2F_{7/2}; M_J=\frac{7}{2})$]. Some typical examples are the number of holes $n_h=w_0^{000}$, the orbital and spin magnetic moments $L_z=lw_0^{101}$ and $S_z=sw_0^{011}$, respectively, and the spin-orbit coupling $\mathbf{L}\cdot\mathbf{S}=-ls w_0^{110}$. Note that the relation for O^{xyz} does not hold for the magnetic dipole operator $T_z=[l/(2l+3)]w_0^{211}$ due to its definition in real instead of angular momentum space.

By summing Eq. (28) over both spin-orbit split edges

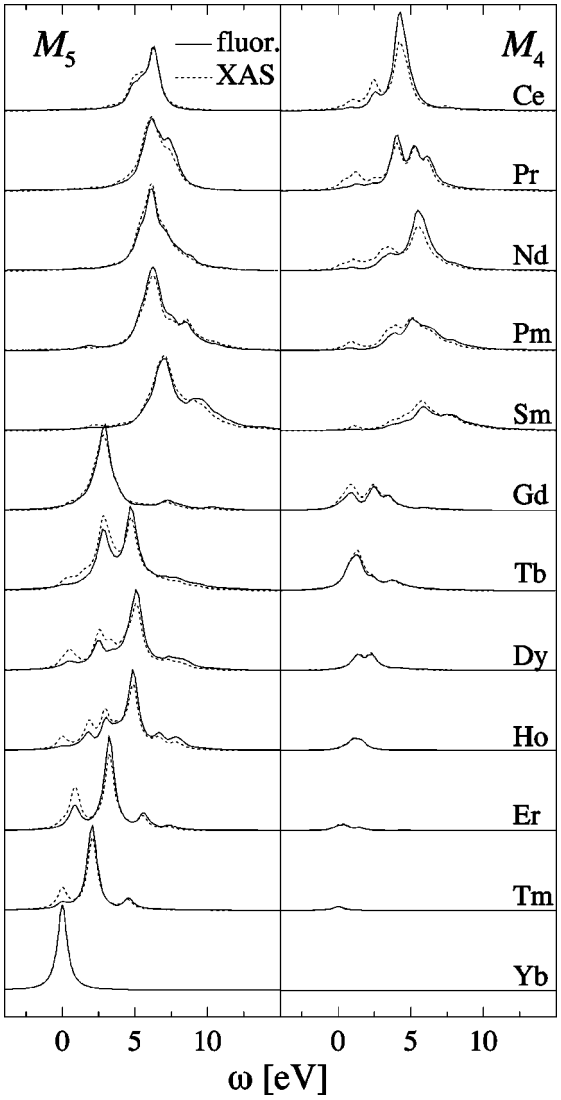

FIG. 3. Isotropic dipolar XAS spectra ($4f^n \rightarrow \underline{3d}4f^{n+1}$, dotted line) and fluorescence spectra for isotropic incoming and outgoing light ($4f^n \rightarrow \underline{3d}4f^{n+1} \rightarrow 4f^n$, solid line) as a function of excitation energy ω for trivalent rare-earth ions. XAS and fluorescence have been normalized to the intensity integrated over both edges; the scaling between spectra for different ions is arbitrary. The left and right panels show the M_5 and M_4 edges, respectively.

$$\overline{I}_0^z(j^+) + \overline{I}_0^z(j^-) = \frac{\langle w_0^{z0z} \rangle}{\langle n_h \rangle} \tag{30}$$

we obtain the sum rule that relates the total integrated intensity to the spin-independent operators.[15] ($\overline{I}$ indicates that the spectra are normalized to the integrated intensity of the isotropic spectrum over both spin-orbit split edges.) For $z=1$ we have the ''L_z'' sum rule. In general, it relates the integrated intensity of $I_0^z(\omega)$ to spin-independent operators that give the 2^z-polar moment in the electron distribution. For $z=0$ it simply says that the integrated intensity over both edges is proportional to the number of holes. For higher values of z the ground state expectation values of w^{z0z} show an oscillatory behavior along the rare-earth series; see Fig. 5. This behavior is already well described by assuming a Hund rule ground state.[30]

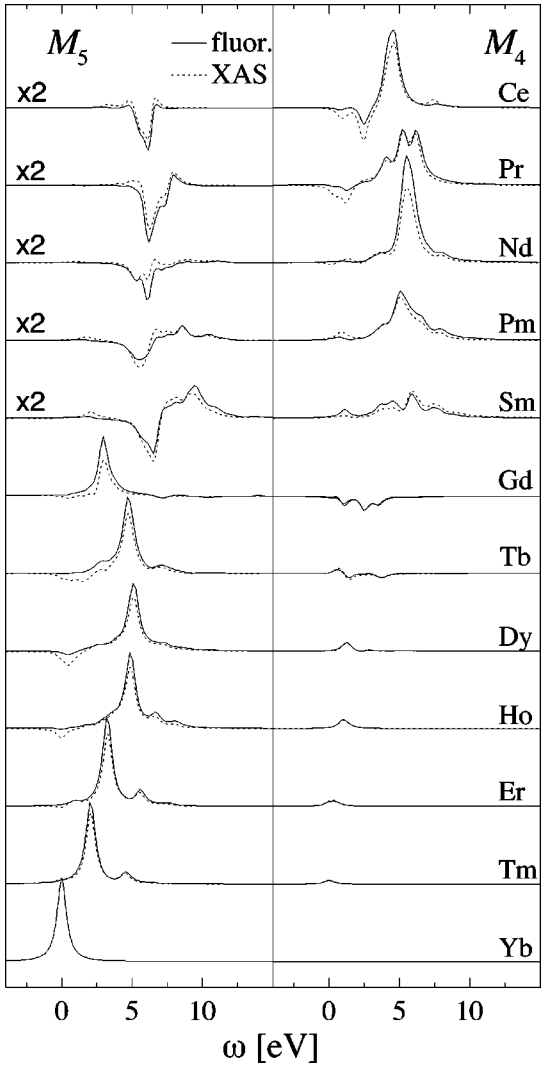

FIG. 4. Same as Fig. 3, but now for left minus right circularly polarized incoming light. Some of the spectra are scaled relative to the spectra of Fig. 3. The scaling applies also to the right panel.

A weighted substraction of both edges can be related to the spin-dependent operators

$$\overline{I_0^z}(j^+)-\frac{c+1}{c}\overline{I_0^z}(j^-)=\frac{1}{\langle n_h\rangle}\left\{\frac{z}{[z]}\langle w_0^{z-1,1,z}\rangle+\frac{z+1}{[z]}\langle w_0^{z+1,1,z}\rangle\right\}; \qquad (31)$$

For $z=0$ this expression forms the basis of the theory of branching ratios.[28] It relates the integrated intensities of the spin-orbit split edges of the isotropic spectrum to the ground state expectation value of the spin-orbit operator (note that $w^{-1,1,0}$ is not defined as a physical operator). For $z=1$ it gives the ''S_z-T_z'' sum rule.[16]

The assumption in deriving this equation is that a certain spin-orbit split edge can be described by the core hole having the corresponding j value. This approximation is valid for late rare earths (and also late transition metals). For early rare earths deviations are found for the spin-dependent sum rule; see Fig. 5. Although for these systems a smaller spin-orbit coupling is found, this is not the dominant effect that

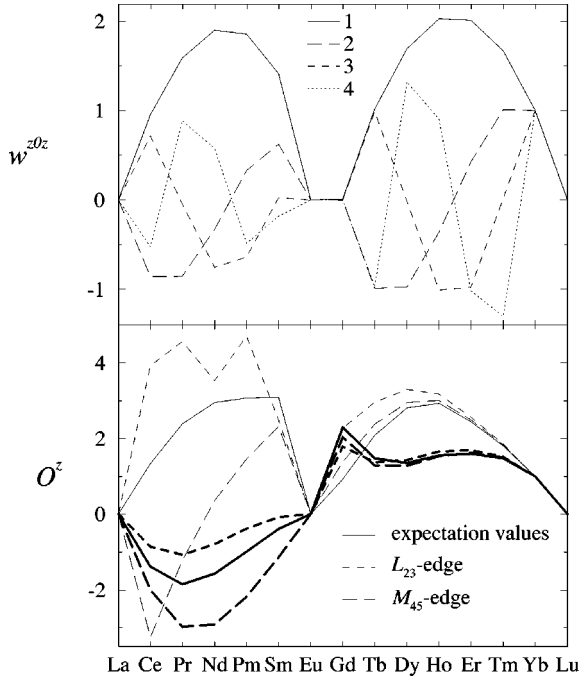

FIG. 5. The upper panel shows the ground state expectation values of w^{z0z} for trivalent rare-earth ions for $z=1$ (solid line), 2 (long-dashed), 3 (dashed), and 4 (dotted). The lower panel shows the ground state expectation value of $O^z=(z/[z])w^{z-1,1,z}+\{(z+1)/[z]\}w^{z+1,1,z}$ (solid line). The dashed and long-dashed lines show $n_h\{I_0^z(j^+)-[(c+1)/c]I_0^z(j^-)\}$ for the L_{23} and M_{45} edges, respectively. This quantity is equal to O^z according to the sum rules; see the text. The thin and thick lines correspond to $z=0$ and 1, respectively.

causes the stronger mixing of the two edges. More important are the LSJ values that are reached by the absorption. For late rare earths the ground state has maximum LSJ values. As a result of the dipole selection rules ($\Delta S=0$ and $\Delta L=0,\pm1$) also high LSJ values for XAS final states are found. These states are predominantly found in the j^+ edge. A qualitative argument for this goes as follows. Within LS coupling (i.e., no spin-orbit coupling) the $\underline{c}l^{n+1}$ states with high LS values have relatively low energies (where $\underline{c}$ indicates a core hole). After switching on the spin-orbit coupling the LS states with low energy predominantly go into the j^+ edge and those with high energy into the j^- edge. Hence, for the states with high LSJ values there is only small mixing between the two edges. The most extreme examples are the states with maximum LSJ values that occur only in the j^+ edge. The limited presence of high LSJ character in the j^- edge directly explains why the L_2 and M_4 edges have little intensity for late rare earths.

The situation is different for early rare earths. First, the total J of the ground state is given by $|L-S|$. Second, for early rare earths the maximum spin of the XAS final states is higher than that of the ground state ($S_n^{\max}=S_g^{\max}+1$).[28] Since in XAS $\Delta S=0$ these states have little weight (as a result of the mixing by the spin-orbit coupling they obtain a finite intensity). For early rare earths excitations therefore occur at intermediate LSJ values. This can also be seen in the M_{45} XAS spectra where for early rare earths significant intensity only occurs at 5–10 eV above the absorption edge (which

consists of the ''dipole-forbidden'' maximum spin states); see Fig. 3. The stronger mixing between the edges is directly apparent from strong intensity at both edges. This mixing has as a result that for early rare earths deviations for the spin-dependent sum rule are found, although for $z=1$ the trends are well predicted.

B. Resonant inelastic x-ray scattering

For x-ray inelastic scattering sum rules one has to integrate over the incoming and outgoing photon energies. Let us first consider the integration over the transferred energy $\Delta\omega=\omega-\omega'$, which leads to a term describing the decay of an intermediate state, $I^{z'}_{\zeta'}(n'n)=\Sigma_f I^{z'}_{\zeta'}(n'ffn)$. Note the presence of cross terms as a result of interference between intermediate states leading to the same final state. For the decay one has to distinguish two situations.

First, the core hole is filled by an electron from a shallower core level, leading to a Raman process described by $l^n\rightarrow\underline{c}l^{n+1}\rightarrow\underline{c}'l^{n+1}$. If both the intermediate and final states are split by the spin-orbit coupling the spectrum has four clearly separated manifolds. For a given manifold we find[30]

$$I^{z'}_{\zeta'}(nn';jj') = \mathcal{B}^{z'}_{jj'}(c,Q,c')\sum_{m,m'}(-1)^{j-m'}\begin{pmatrix} j & z' & j \\ -m' & \zeta' & m\end{pmatrix} \times\langle n'|c_{jm'}c^{\dagger}_{jm}|n\rangle n^{-1}_{jz'}, \tag{32}$$

with the coefficient given by

$$\mathcal{B}^{z'}_{jj'}(c,Q,c')=(-1)^{j+j'+c+c'}P^2_{cc'}[jj']\begin{Bmatrix} j & j' & Q' \\ c' & c & s\end{Bmatrix}^2 \times\begin{Bmatrix} Q' & Q' & j' \\ j & j & z'\end{Bmatrix}n_{jz'}n^{-1}_{Q'z'}. \tag{33}$$

The decay of an intermediate state ($n=n'$) is therefore determined by an expectation value of the polarization of the core hole for that state. For, e.g., $z'=1$ this expectation value is $\langle j_z\rangle$.

Let us consider a specific example. A typical resonant Raman process[9,10] is given by $l=4f$, $c=2p$, and $c'=3d$. For simplicity we take the incoming light to be isotropic. If the system is magnetic the absorption process still creates a polarized core hole as a result of the polarization of the valence shell. If the polarization is not detected the outgoing light has an isotropic and linear dichroic part [see Eq. (23)]

$$\frac{1}{2}\{I(\omega,\hat{\mathbf{k}}'\boldsymbol{\epsilon}^+\omega')+I(\omega,\hat{\mathbf{k}}'\boldsymbol{\epsilon}^-\omega')\} = \frac{2\pi}{\hbar}N_{\omega'}N_{\omega}B_1^2B_2^2 i\left\{I_0^{000}(\omega,\omega')+\frac{1}{2}C_0^2(\hat{\mathbf{k}})I_0^{022}(\omega,\omega')\right\}. \tag{34}$$

Figure 6 gives the two different spectra for Ho^{3+} at three different incoming photon energies. If we now take, for a certain absorption energy, the difference of two spectra at different detection angles with respect to the magnetic axis, we obtain a signal that is proportional to $I_0^{022}(\omega,\omega')$. In that case the integration over ω' of a spectrum at a given absorption energy is finite at the L_3 edge, but zero at the L_2 edge; see Fig. 6. This is a direct result of the fact that the $j=\frac{1}{2}$ level has no quadrupolar moment (a finite intensity can still occur as a result of the presence of $j=\frac{3}{2}$ character in the L_2 edge due to the mixing by the core-valence Coulomb interactions).

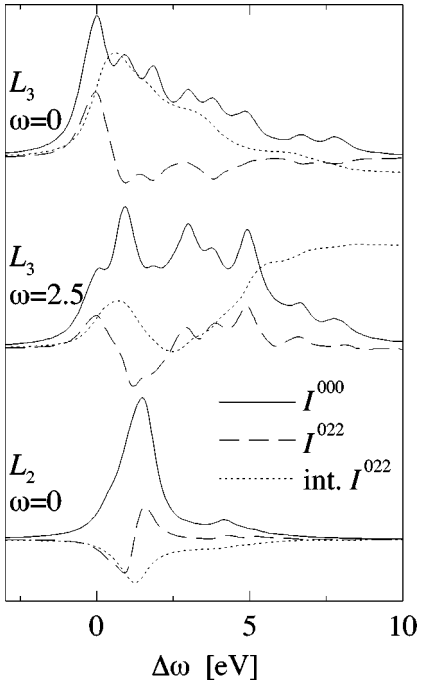

FIG. 6. RIXS spectra ($4f^n\rightarrow\underline{2p}4f^{n+1}\rightarrow\underline{3d}4f^{n+1}$) as a function of transferred energy $\Delta\omega=\omega-\omega'$. The zero of the energy scale corresponds to the energy of the lowest final state of a certain edge. Spectra are given at three excitation energies, from top to bottom: at the L_3 absorption edge, 2.5 eV above the L_3 absorption edge, and at the L_2 absorption edge; see Fig. 1. Only the M_5 edge is shown. The incoming light is isotropic; the outgoing light is isotropic [$I_0^{000}(\omega,\omega')$, solid line] and linear dichroic [$I_0^{022}(\omega,\omega')$, dashed line]. The dotted line gives the intensity of $I_0^{022}(\omega,\omega')$ integrated along the $\Delta\omega$ axis.

For a measurement with isotropic outgoing light the expectation value is proportional to $\delta_{n,n'}$, i.e., the decay is constant and all interference terms cancel. When a summation over both j' edges is made one obtains[18,30]

$$I_0^{z'=0}(nn')=\sum_{j'}I_0^0(nn';jj')=\frac{P^2_{cc'}}{[c]}\delta_{n,n'}. \tag{35}$$

Therefore, for isotropic outgoing light an integration over the transferred energy $\omega-\omega'$ leads to a spectrum as a function of excitation energy ω that is proportional to XAS.[18,30]

The second case is where the deexcitation involves the valence shell, i.e., $l^n\rightarrow\underline{c}l^{n+1}\rightarrow l^n$. Figures 3 and 4 show the spectra integrated over the energy of the outgoing photons (fluorescence yield) for isotropic and circular dichroic incoming light, respectively; the outgoing light has been taken to be isotropic. We observe significant differences with the XAS spectra. Therefore, even for isotropic outgoing light,

the decay cannot be decoupled from the excitation. In contrast to Eq. (32), where the operators working on the closed shell could be removed, one obtains here that the decay is proportional to an intermediate-state expectation value of a two-particle operator. For isotropic outgoing light one has[19]

$$I_0^{z'=0}(nn')=\frac{P_{cl}^2}{[c]}\Bigg\{\delta_{n,n'}+\frac{1}{[l]n_{l1c}^2}\sum_{\lambda,\lambda',\gamma,\gamma',\sigma,\sigma'}\delta_{\lambda'-\gamma',\lambda-\gamma}\times c^1(c\gamma',l\lambda')c^1(c\gamma,l\lambda)\times\langle n'|l_{\lambda\sigma}c_{\gamma'\sigma'}l^\dagger_{\lambda'\sigma'}c^\dagger_{\gamma\sigma}|n\rangle\Bigg\}, \tag{36}$$

where $c^1(c\gamma,l\lambda)$ are the Slater-Condon parameters.[33] The matrix elements are, except for an offset and the radial integrals, equivalent to those of the G^1_{cl} Coulomb exchange. Note that the ''G^1_{cl}'' term also assumes negative values and that the lowest possible value for $I_0^{z'=0}$ is zero. The G^1_{cl} Coulomb term is also for a large part responsible for the position of the eigenstates in a spin-orbit manifold. This directly explains the trend in the fluorescence spectra, that the states closer to the absorption threshold in a certain edge have in general a smaller decay compared to those at the high-energy side of an edge.

Let us now consider the sum rules for the intensities integrated along the transferred and excitation energy. For deep-lying core levels with a large lifetime broadening, such as the $2p$ shell, one can use the fast-collision approximation.[17,18] This implies replacing the intermediate-state energy denominator by $\overline{\mathcal{E}_n}=\omega+E_g-\overline{E_n}+i(\Gamma/2)$, where $\overline{E_n}$ is an average energy. For the situation where the emission involves two core levels one can then derive[18,30]

$$I_0^{zz'r}(j,j')=\int_j d\omega\int_{j'}d\omega' I_0^{zz'r}(\omega,\omega')$$

$$=\mathcal{B}^{z'}_{jj'}(c,Q,c')\sum_{x,y}\mathcal{C}_j^{xyrzz'}(c,Q,l)\langle w_0^{xyr}\rangle, \tag{37}$$

where the coefficients $\mathcal{B}$ and $\mathcal{C}$ are given in Ref. 30. For isotropic outgoing light we have $\mathcal{C}_j^{xyzz0}=(P_{cl}^2/[cl])M_y(j)N_{xyz}$, which means that the same coefficients are found as for XAS. In this limit the fast-collision approximation is not necessary since all interference effects cancel.

When the deexcitation involves the valence states the situation is more complex. Sum rules would involve two-particle valence shell expectation values that are difficult to evaluate. Recently, an investigation has been made into the applicability of XAS, sum rules for spectra obtained with fluorescence yield,[19] which is applicable when the Auger lifetimes are not too strongly term dependent. Although fluorescence yield is in principle not equal to XAS the conditions for integrated intensities are less stringent. Here one does not require that every final state has a constant decay but that the total decay of the excited intermediate states does not have a strong polarization dependence.

The state after excitation with q-polarized light can be written as $|v_q\rangle=\Sigma_n a_n(q)|n\rangle$; this state can be normalized to unity by using the coefficients $\overline{a}_n(q)=a_n(q)/\sqrt{\langle v_q|v_q\rangle}$. The integrated intensity of the fluorescence spectrum excited with q-polarized light can then be written as[19]

$$I_q^{\rm fluor}=\langle v_q|v_q\rangle\langle V^\Gamma\rangle_q=I_q^{\rm XAS}\langle V^\Gamma\rangle_q, \tag{38}$$

i.e., the integrated intensity is given by the XAS intensity multiplied by a term that describes the radiative decay. If the polarization of the outgoing light is not measured this latter term is given by

$$\langle V^\Gamma\rangle_q=\sum_{z'\ \rm even}\mathcal{T}_{z'}C_0^{z'}(\hat{\mathbf{k}}')\sum_{n,n'}\frac{\pi}{\Gamma}\frac{\overline{a}_n\overline{a}_{n'}}{\left(\frac{E_n-E_{n'}}{\Gamma}\right)^2+1}I_0^{z'}(nn'). \tag{39}$$

This clearly shows that the total decay for q-polarized light $\langle V^\Gamma\rangle_q$ is a weighted average of the decays of the intermediate states $I_0^{z'}(nn')$. Proportionality of the integrated intensity of the circular dichroic fluorescence spectra, i.e., $(\Sigma_q qI_q^{\rm fluor})/(\Sigma_q I_q^{\rm fluor})$, with $\langle w^{101}\rangle=\langle L_z\rangle/l$ is obtained if $\langle V^\Gamma\rangle_q$ is not strongly dependent on the polarization. Numerical evaluation of $\langle V^\Gamma\rangle_q$ shows that this situation is found for early rare earths, but that there is a strong polarization dependence for late rare earths.[19] This can be understood as follows. As was shown above, the decay of the intermediate states is proportional to a ''G^1_{cl}''-like term. Maximum variations in decay can be expected for ''pure'' LS-like intermediate states. The effect of mixing by the spin-orbit coupling is small for the high LSJ states that are reached in absorption in late rare earths, leading to a strong polarization dependence. The stronger mixing of the intermediate LSJ states that are reached in early rare earths decreases variations in $\langle V^\Gamma\rangle_q$. It is remarkable that the mechanism that causes deviations for the ''S_z'' XAS sum rule improves the agreement between L_z values obtained by fluorescence yield and the ground state expectation values.

It must be noted that a more efficient way to remove variations in $\langle V^\Gamma\rangle_q$ is to create a $|v_q\rangle$ that has not a strong LS-like character. This is found for many transition-metal systems where a strong crystal field quenches the orbital moment.

V. CONCLUSION

In conclusion, a comparison has been made between XAS and resonant inelastic x-ray scattering. Several aspects deserve further experimental investigation. The isotropic L_{23} spectra should be reexamined since, as was shown by Loeffen *et al.*,[11] more detailed information can be obtained by partial deconvolution of the lifetime broadening. This should enable a direct comparison of the relative size of the dipolar and quadrupolar contributions. Also a careful determination of the intensities of the two spin-orbit split edges would be interesting. It is generally assumed that for isotropic light $I^0_{L_3}/I^0_{L_2}=2{:}1$. However, a strong polarization of the $5d$ electrons in the ground state would give deviations from the statistical branching ratio.

The experimental developments in x-ray inelastic scatter-

ing are more recent. It is now rather well established that on resonance the excitation and decay cannot be decoupled. For a delocalized system this implies that one has to take into account the crystal momentum of the core hole (although core-valence interactions in the intermediate state might change its value). For a localized system one has to consider the angular momentum. Within an independent electron model the angular momentum is conserved. However, interactions with the valence shell change the values of j and m and in general for an intermediate-state eigenstate one has to consider expectation values of, e.g., j_z of the core hole. This quantity could be obtained, e.g., by measuring the difference between left and right circular polarization of the outgoing light. Unfortunately, these experiments are rather complex. A determination of the quadrupolar moment of the core hole polarization seems more promising since it involves a measurement at two different detection angles. The presence of core-hole polarization has been demonstrated in resonant photoemission[34] ($l^n \rightarrow \underline{c} l^{n+1} \rightarrow \underline{c}'^2 l^{n+1} E_k$, where E_k denotes a photoelectron), which is formally very similar to the scattering process $l^n \rightarrow \underline{c} l^{n+1} \rightarrow \underline{c}' l^{n+1}$. Recent resonant Raman experiments on Co show the presence of higher moments in the core hole distribution.[35]

The x-ray scattering process $l^n \rightarrow \underline{c} l^{n+1} \rightarrow l^n$ enables one to study valence band excitations. Although for electric multipole transitions $\Delta S = 0$, these excitations also include spin flips since the spin is not a good quantum number in the intermediate state as a result of the large core-hole spin-orbit coupling. Recently, octet-sextet transitions have been observed in Gd^{3+} (ground state $^8S_{7/2}$).[36]

A relatively simple way to study resonant inelastic x-ray scattering is fluorescence yield since it does not involve the detection of the energy of the outgoing photon. The spectra for fluorescence yield already show significant deviations from the XAS cross section.

*Present address: Materials Science Division, Argonne National Laboratory, 9700 South Cass Avenue, Argonne, IL 60439.

[1] G. Schütz, W. Wagner, W. Wilhelm, P. Kienle, R. Zeller, R. Frahm, and G. Materlik, Phys. Rev. Lett. **58**, 737 (1987).

[2] G. van der Laan, B. T. Thole, G. A. Sawatzky, J. B. Goedkoop, J. C. Fuggle, J.-M. Esteva, R. C. Karnatak, J. P. Remeika, and H. A. Dabkowska, Phys. Rev. B **34**, 6529 (1986).

[3] D. Gibbs, D. R. Harshman, E. D. Isaacs, D. B. McWhan, D. Mills, and C. Vettier, Phys. Rev. Lett. **61**, 1241 (1988).

[4] J. P. Hannon, G. T. Trammell, M. Blume, and D. Gibbs, Phys. Rev. Lett. **61**, 1245 (1988).

[5] P. Carra and M. Altarelli, Phys. Rev. Lett. **64**, 1286 (1990).

[6] P. Carra, B. N. Harmon, B. T. Thole, M. Altarelli, and G. A. Sawatzky, Phys. Rev. Lett. **66**, 2495 (1991).

[7] X. D. Wang, T. C. Leung, B. N. Harmon, and P. Carra, Phys. Rev. B **47**, 9087 (1993); J. C. Lang, S. W. Kycia, X. D. Wang, B. N. Harmon, A. I. Goldman, D. J. Branagan, R. W. McCallum, and K. D. Finkelstein, *ibid.* **46**, 5298 (1992).

[8] P. Fischer, G. Schütx, S. Stähler, and G. Wiesinger, J. Appl. Phys. **69**, 6144 (1991); K. Shimomi, H. Maruyama, K. Kobayashy, A. Koizumi, H. Yamazaki, and T. Iwazumi, Jpn. J. Appl. Phys., Part 1 **32-2**, 314 (1992); J. C. Lang, G. Strajer, C. Detlefs, A. I. Goldman, H. König, X. Wang, B. N. Harmon, and R. W. McCallum, Phys. Rev. Lett. **74**, 4935 (1995).

[9] K. Hämäläinen, D. P. Siddons, J. B. Hastings, and L. E. Berman, Phys. Rev. Lett. **67**, 2850 (1991).

[10] M. H. Krisch, C. C. Kao, F. Sette, W. A. Caliebe, K. Hämäläinen, and J. B. Hastings, Phys. Rev. Lett. **74**, 4931 (1995).

[11] P. W. Loeffen, R. F. Pettifer, S. Müllender, M. van Veenendaal, J. Röhler, and D. S. Sivia, Phys. Rev. B **54**, 14 877 (1996).

[12] B. N. Harmon and A. J. Freeman, Phys. Rev. B **10**, 1979 (1974).

[13] T. Jo and S. Imada, J. Phys. Soc. Jpn. **62**, 3721 (1993).

[14] M. van Veenendaal, J. B. Goedkoop, and B. T. Thole, Phys. Rev. Lett. **78**, 1162 (1997); J. Electron Spectrosc. Relat. Phenom. **86**, 151 (1997).

[15] B. T. Thole, P. Carra, F. Sette, and G. van der Laan, Phys. Rev. Lett. **68**, 1943 (1992).

[16] P. Carra, B. T. Thole, M. Altarelli, and X. Wang, Phys. Rev. Lett. **70**, 694 (1993).

[17] J. Luo, G. T. Trammell, and J. P. Hannon, Phys. Rev. Lett. **71**, 287 (1993).

[18] P. Carra, M. Fabrizio, and B. T. Thole, Phys. Rev. Lett. **74**, 3700 (1995).

[19] M. van Veenendaal, J. B. Goedkoop, and B. T. Thole, Phys. Rev. Lett. **77**, 1508 (1996).

[20] A. I. Akhiezer and V. B. Berestetsky, *Quantum Electrodynamics* (Consultants Bureau, New York, 1957); J. P. Hannon and J. P. Trammel, Phys. Rev. **186**, 306 (1969); P. Carra and B. T. Thole, Rev. Mod. Phys. **66**, 1509 (1994).

[21] D. M. Brink and G. R. Satchler, *Angular Momentum* (Oxford University Press, Oxford, 1968).

[22] B. T. Thole and G. van der Laan, Phys. Rev. B **49**, 9613 (1994).

[23] D. A. Varshalovich, A. N. Moskalev, and V. K. Khersonskii, *Quantum Theory of Angular Momentum* (World Scientific, Singapore, 1988).

[24] R. D. Cowan, *The Theory of Atomic Structure and Spectra* (University of California Press, Berkeley, 1981).

[25] B. T. Thole, G. van der Laan, J. C. Fuggle, G. A. Sawatzky, R. C. Karnatak, and J.-M. Esteva, Phys. Rev. B **32**, 5107 (1985).

[26] J. B. Goedkoop, B. T. Thole, G. van der Laan, G. A. Sawatzky, F. M. F. de Groot, and J. C. Fuggle, Phys. Rev. B **37**, 2086 (1988).

[27] S. Imada and T. Jo, J. Phys. Soc. Jpn. **59**, 3358 (1990).

[28] B. T. Thole and G. van der Laan, Phys. Rev. A **38**, 1943 (1988); Phys. Rev. B **38**, 3158 (1988).

[29] B. T. Thole, G. van der Laan, and M. Fabrizio, Phys. Rev. B **50**, 11 466 (1994).

[30] M. van Veenendaal, P. Carra, and B. T. Thole, Phys. Rev. B **54**, 16 010 (1996). Note that here, of the reduced matrix elements P_{cl}, only $[cl]^{1/2}$ is maintained.

[31] B. R. Judd, *Second Quantisation in Atomic Spectroscopy* (Johns Hopkins University Press, Baltimore, 1967).

[32] P. Carra, H. König, B. T. Thole, and M. Altarelli, Physica B **192**, 182 (1993).

[33] E. U. Condon and G. H. Shortley, *The Theory of Atomic Spectra* (Cambridge University Press, Cambridge, 1951).

[34] B. T. Thole, H. A. Dürr, and G. van der Laan, Phys. Rev. Lett. **74**, 2371 (1995).

[35] L. Braicovich *et al.* (unpublished).

[36] C. Dallera, L. Braicovich, C. Chiringhelli, M. van Veenendaal, J. B. Goedkoop, and N. B. Brookes, Phys. Rev. B **56**, 1279 (1997).